AGU PUBLICATIONS

Geophysical Research Letters

RESEARCH LETTER
10.1002/2015GL065273

Key Points:
- We obtained in situ visible-NIR reflectance spectra of the lunar surface at Chang'E-3 landing site
- These in situ spectra have less mature features than that measured remotely
- Using the spectral lookup table, we identified large amount of olivines

Supporting Information:
- Texts S1 and S2, Figures S1–S5, and Tables S1–S4

Correspondence to:
H. Zhang,
um_zhanghao@yahoo.com

Citation:
Zhang, H., et al. (2015), In situ optical measurements of Chang'E-3 landing site in Mare Imbrium: 1. Mineral abundances inferred from spectral reflectance, *Geophys. Res. Lett.*, *42*, 6945–6950, doi:10.1002/2015GL065273.

Received 8 JUL 2015
Accepted 12 AUG 2015
Accepted article online 18 AUG 2015
Published online 10 SEP 2015

In situ optical measurements of Chang'E-3 landing site in Mare Imbrium: 1. Mineral abundances inferred from spectral reflectance

Hao Zhang[1], Yazhou Yang[1], Ye Yuan[1], Weidong Jin[1], Paul G. Lucey[2], Meng-Hua Zhu[3], Vadim G. Kaydash[4], Yuriy G. Shkuratov[4], Kaichang Di[5], Wenhui Wan[5], Bin Xu[5], Long Xiao[1], Ziwei Wang[1], and Bin Xue[6]

[1]Planetary Science Institute, School of Earth Sciences, China University of Geosciences, Wuhan, China, [2]Hawaii Institute of Geophysics and Planetology, University of Hawaii, Honolulu, Hawaii, USA, [3]Space Science Institute, Macau University of Science and Technology, Taipa, China, [4]Astronomical Institute, Kharkov V.N. Karazin National University, Kharkov, Ukraine, [5]State Key Laboratory of Remote Sensing Science, Institute of Remote Sensing and Digital Earth, Chinese Academy of Sciences, Beijing, China, [6]Xi'an Institute of Optics and Precision Mechanics, Chinese Academy of Sciences, Xi'an, China

Abstract The visible and near-infrared imaging spectrometer on board the Yutu Rover of Chinese Chang'E-3 mission measured the lunar surface reflectance at a close distance (~1 m) and collected four spectra at four different sites. These in situ lunar spectra have revealed less mature features than that measured remotely by spaceborne sensors such as the Moon Mineralogy Mapper instrument on board the Chandrayaan-1 mission and the Spectral Profiler on board the Kaguya over the same region. Mineral composition analysis using a spectral lookup table populated with a radiative transfer mixing model has shown that the regolith at the landing site contains high abundance of olivine. The mineral abundance results are consistent with that inferred from the compound measurement made by the on board alpha-particle X-ray spectrometer.

1. Introduction

The chemical, mineral, and physical properties of the lunar surface carry information regarding the geological history and space environment of the Moon [e.g., *Lucey et al.*, 2006]. Currently, it is believed that the abundance and spatial distributions of the dominant minerals of mare basalts including olivine (OLV), clinopyroxene (CPX), orthopyroxene (OPX), plagioclase (PLG), and ilmenite are determined by a global fractionation event of magma ocean induced flotation of anorthosite-rich crust and the subsequent magmatism of basalts derived from melting of the mantle [*Staid and Pieters*, 2001]. Thus, the accurate mapping and validations of mineral types, distributions, and abundance play a key role in understanding the evolutionary history of the Moon.

Visible and near-infrared spectroscopy is a powerful tool in remote characterizations of the physical and mineralogical properties of the Moon [e.g., *Shkuratov et al.*, 2011]. However, there is a large gap in spatial scale between spectral measurements from orbit with resolutions at best of tens to hundreds of meters and the spectral properties of individual samples returned from the Moon and analyzed in terrestrial laboratories [*Ohtake et al.*, 2013; *Pieters et al.*, 2013; *Donaldson Hanna et al.*, 2014]. The successful landing of the Chang'E-3 (CE3) lander and the deployment of the Yutu Rover at Mare Imbrium [*Xiao et al.*, 2015] has provided the first in situ spectral analysis of the lunar surface. The Visible and Near-infrared Spectrometer (VNIS) on board the rover captured the spectral features of the lunar surface at centimeter to meter scales that can bridge this gap in scales to help us better understand the lunar environment and evolutionary history.

2. Instrument, Measurement, and Data Reductions

The VNIS and the Active Particle X-ray Spectrometer (APXS) instruments are located on the lower left and lower right on the front surface of the rover, respectively. The VNIS is located about 0.7 m above the ground and looks down at the lunar surface at a nominal 45° angle and roughly images an area of 13 by 13 cm (Figure S1 in the supporting information). The APXS detector is situated at a robotic arm and looks at the lunar surface at a distance of 20 mm. The VNIS consists of a Complementary Metal-Oxide Semiconductor (CMOS) imager with 256 by 256 pixels and a short-wavelength near-infrared (SWIR) detector with one-single pixel [*Liu et al.*, 2014] using acousto-optic tunable filters for wavelength discrimination. The CMOS camera spans the wavelength

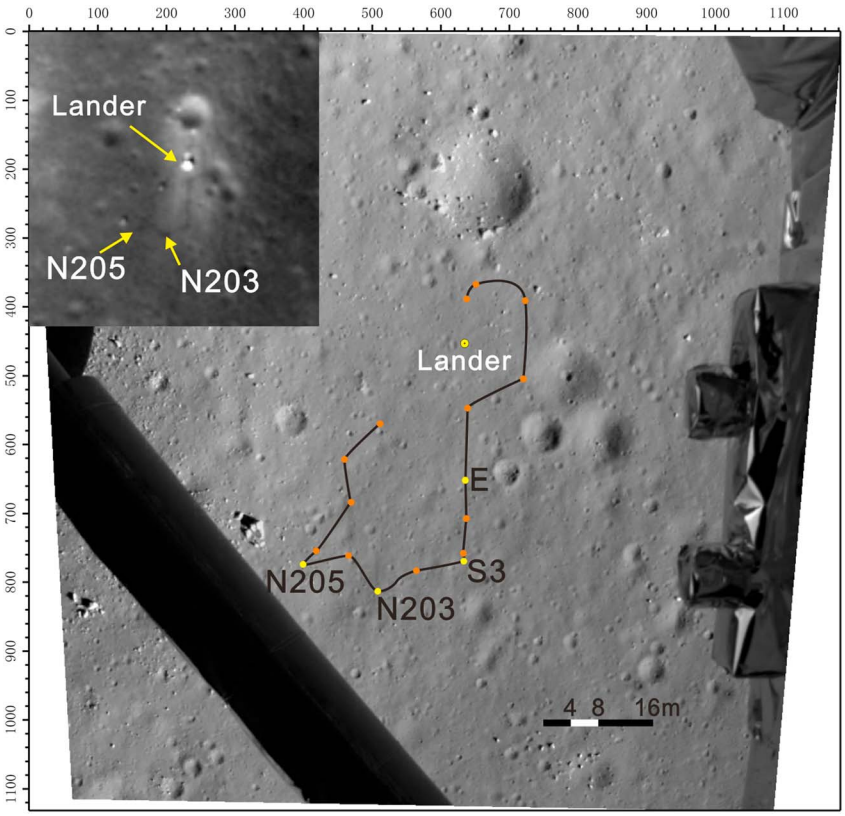

Figure 1. Orthorectified image of the landing area taken by the Landing Camera. The landing site is marked by the yellow dot (Lander), and the rover's path with locations of the four VNIS measurements is also marked. The inset is a Lunar Reconnaissance Orbiter Camera image taken on 17 February 2014 showing the increased surface albedo after landing.

range from 450 to 945 nm with a spectral resolution of 2–7 nm, and the SWIR detector works from 900 to 2395 nm with a spectral resolution of 3–12 nm, respectively, and both operate at 5 nm spectral sampling. The single-pixel SWIR detector images a circled area within the field of view of the CMOS camera (Figure S1). The typical signal-to-noise ratios of the CMOS and SWIR sensors are better than 30 dB (1000:1) when making measurements in the typical lunar environment (*Report of Scientific Validations of Visible-Near-infrared Imaging Spectrometer of the Chang'E 3 Mission*, Document # CE3-GRAS-CSSY-003-F3, version 1.0, Released 16 May 2012).

As indicated in Figure 1, the Yutu rover path is roughly a flipped L shape. The VNIS collected individual spectra at four different sites (Nodes E, S3, N203, and N205), from 23 December 2013 to 14 January 2014 (see Table S1 for measurement locations and times). The calibrated radiance values ($\mu Wcm^{-2}Sr^{-1}\,nm^{-1}$) were provided by the payload team after performing dark current subtractions and several multiplicative corrections including flat field, geometric corrections, and radiometric calibration. Reflectance expressed in terms of the reflectance factor [*Hapke*, 2012] was obtained by using the solar irradiance calibration method (see supporting information (SI)). In addition, two APXS measurements were also made at Node S3 and Node N205 and the results are summarized in Table 1.

Figure 2 displays the VNIS reflectance spectra with photometric corrections which bring the reflectance to the NASA Reflectance Experiment Laboratory configuration ($i = 30°$, $e = 0°$) (SI). To compare the in situ data with remote measurements made over the same region, we also plot 25 reflectance spectra measured by the Chandrayaan-1 Moon Mineralogy Mapper (M^3) [*Pieters et al.*, 2009] (http://pds-imaging.jpl.nasa.gov/data/m3/CH1M3_0004/DOCUMENT/DPSIS.PDF. It should be noted that the M^3 level 2 data product released is actually the radiance factor which should be divided by the cosine of the incident zenith to obtain the reflectance defined in equation (S2)). These 25 pixels form a 5 by 5 "matrix" with its central element (element [3, 3]) being centered on the location of the CE3 lander. Since each M^3 pixel has a spatial resolution of 140 m, the total area

Table 1. Elemental Abundance Results From the Two APXS Measurements Made at Node S3 and Node N205

	Node S3		Node N205	
Components	Wt (%)	Fit Err (%)	Wt (%)	Fit Err (%)
MgO	10.503	7.487	10.116	6.037
Al_2O_3	10.311	2.325	10.725	2.267
SiO_2	41.882	2.666	40.456	2.934
K_2O	0.131	8.477	0.144	9.260
CaO	10.753	0.336	11.125	0.274
TiO_2	4.173	0.395	4.395	0.244
FeO	21.247	1.037	22.038	0.863

covered by these 25 pixels is roughly a square of 700 by 700 m. In Figure 2, we also plot Kaguya's Spectral Profiler (SP) measurements of a nearby site with center latitude 44.162°N and center longitude 340.514°E. The level 3 SP product is the bidirectional reflectance [*Yamamoto et al.*, 2011]; and thus, it is multiplied by $\pi/\cos(30°)$ to be converted to the reflectance factor [*Hapke*, 2012].

It is seen that all CE3 spectra have deeper 1 μm absorption band, and even the darkest CE3 spectrum, Node N205, is nearly 3 times brighter than the average M^3 spectrum. There are several possible reasons. First, during the landing process, the descent engines should blow away the topmost regolith layers, destruct the intricate "fairy castle" structure of natural soils [*Pieters et al.*, 2013], and expose grains underneath the most weathered surface. Therefore, the VNIS may have measured less mature and less weathered fresh ejecta regolith. Second, as shown by the Lunar Reconnaissance Orbiter Camera (the inset of Figure 1), CE3 was landed near a 450 m diameter fresh crater and the ejecta covers all the path of CE3 rover [*Xiao et al.*, 2015]. Additionally, the CE3 used our in situ phase curve [*Jin et al.*, 2015; W. Jin et al., "In situ optical measurements of Chang'E-3 landing site in Mare Imbrium: 2. Photometric properties of the regolith", submitted to, *Geophysical Research Letters*, 2015] measured nearby to perform the photometric function (equation (S5)) while the M^3 used an empirical phase function derived from highland terrains [*Besse et al.*, 2013] and thus the CE3 spectra should be reliable for the landing site. However, the data reduction pipeline differences should not affect the depth of the measured absorption bands, suggesting a physical difference between the surfaces measured by CE3 and M^3. Despite these differences, the in situ measurements can serve as the ground-truth validations of the future orbital measurements, and analysts are challenged to understand the discrepancies.

3. Mineral Abundance Extractions

There are several approaches to assess mineral compositions of the lunar surface using reflectance spectroscopy [e.g., *Lucey*, 2004; *Noble et al.*, 2006]. To extract mineral abundances, we constructed a synthesized lunar spectral mineral lookup table (LUT) using a radiative transfer model generated in the following steps [*Lucey*, 2004; *Denevi et al.*, 2008; *Lucey et al.*, 2014]. First, optical properties of the grains were computed using an empirical expression that is a function of mineral optical constants which, in turn, are empirical functions of the ratio of Mg to Mg + Fe (Mg number) on a molecular basis. Second, values of single-scattering albedo were computed based on a simplified slab scattering model. Then a one-term Henyey-Greenstein phase function was employed to compute particle single-scattering contributions; the multiple scattering contributions were approximated by the Chandrasekhar H function and added to obtain the total surface reflectance. The effective grain size was fixed to be 17 μm as a study using the Lunar Soil Characterization Consortium data has shown this value is representative [*Pieters et al.*, 1993]. The Mg number was fixed to be 65 [*Lucey et al.*, 2014]. Submicroscopic iron is added to the grains to simulate space

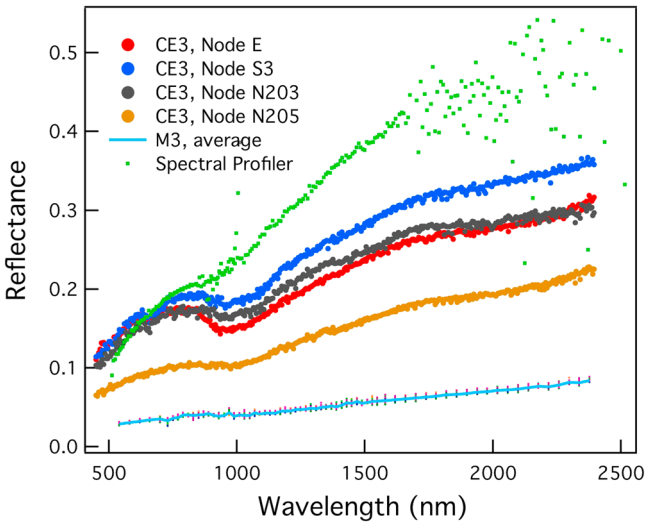

Figure 2. VNIS spectra measured by CE3 and comparisons with M^3 data measured over the landing site. See text for descriptions of the individual M^3 data.

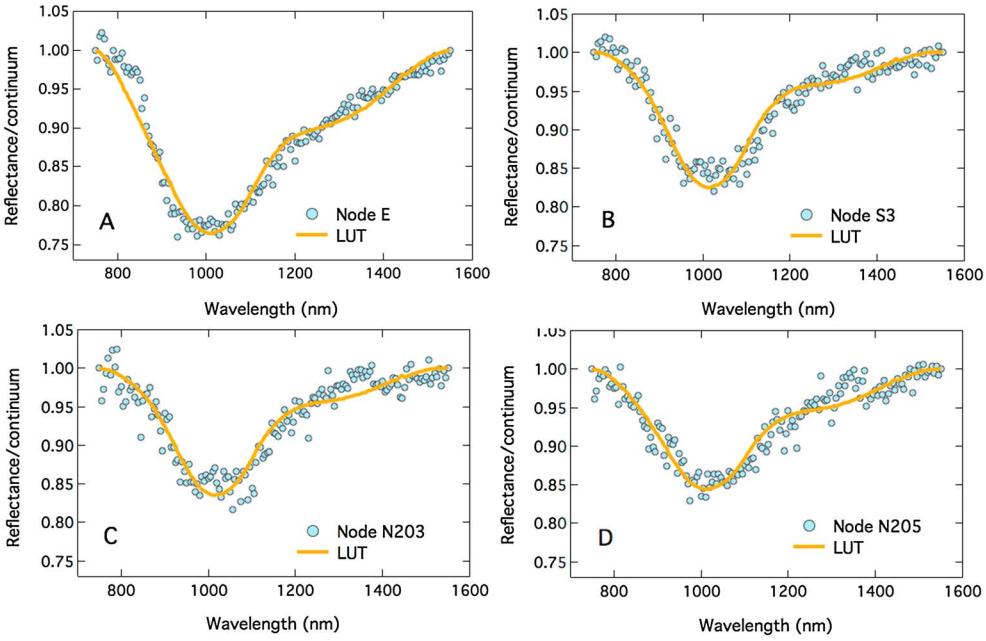

Figure 3. Comparisons of continuum-removed measurement spectra (blue dots) with LUT spectra by searching the minimum absolute difference between them. (a) Node E, (b) Node S3, (c) Node N203, and (d) Node N205.

weathering effects. Since the model used is only valid from 750 to 1550 nm, we confined our analysis to that range [*Lucey et al.*, 2014]. The comparisons were done after removing the continuum background which is estimated as a line connecting the reflectance values at these two positions.

To find the best matches between the LUT and the measurement, we employed four different fitting metrics and used their average as the final matching results (SI). The typical best matches of CE3 measurements and the corresponding LUT spectra are shown in Figure 3, and the corresponding mineral abundances are summarized in Table 2. These results indicate that the landing site is enriched in OLV (13–26 wt %) as compared with the average values of returned mare samples [*Lucey et al.*, 2006]. These mineral abundances are supported by the measurements of the onboard Active Particle X-ray Spectrometer (APXS) at Nodes S3 and N205 (Table 1). The APXS measurements show that the compositions at these two locations have FeO (~22 wt %), TiO_2 (~4 wt %), MgO (~10 wt %), and K_2O (~0.14 wt %), corresponding to OLV ~ 19 wt %, pyroxenes (PXY) ~40 wt %, PLG ~30 wt %, ilmenite ~7 wt % based on CIPW normative mineralogy calculations.

4. Discussion and Conclusions

Figure 4 shows a larger-scale view of the landing area measured by the M^3 instrument. It is seen that the CE3 landing site is within a high-titanium (high-Ti) unit but is very close to the border of the high-Ti and a low-Ti units [*Thiessen et al.*, 2014]. Stratigraphy analysis shows that the younger high-Ti unit covers the low-Ti unit [*Staid et al.*, 2011; *Zhao et al.*, 2014]. To understand the neighboring unit mineralogy, we extracted the SWIR spectra of three representative units indicated in Figure 4: a low-Ti unit (yellow square L), a high-Ti unit (white square H), and a 450 m crater C. These three SWIR spectra are then compared against the mineral LUT,

Table 2. Retrieved Mineral Abundance (wt %) by Comparing CE3 Data and the Mineral Lookup Table Data[a]

Data	OLV	OPX	CPX	PLG	*i* (deg)	*e* (deg)	α (deg)
Node E	26 ± 3	8 ± 5	30 ± 1	31 ± 8	59.90	48.17	107.94
Node S3	15 ± 1	7 ± 1	56 ± 4	17 ± 6	67.50	47.41	85.61
Node N203	13 ± 5	8 ± 0	63 ± 7	11 ± 02	69.70	47.09	86.00
Node N205	23 ± 1	15 ± 0	38 ± 1	19 ± 2	54.05	44.40	95.29

[a]The details that derived these results are given in Table S2 and Figure S4. *i:* solar zenith angle; *e:* sensor zenith angle; and α: phase angle.

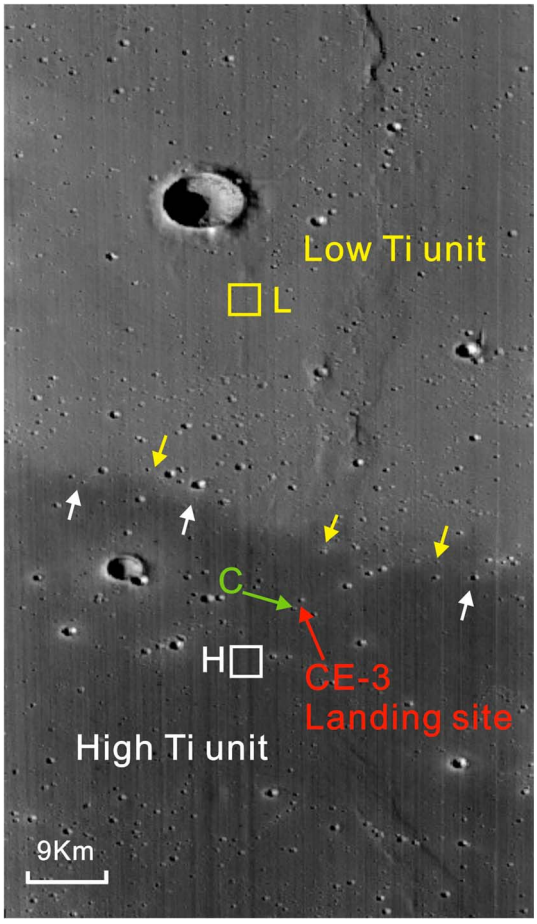

Figure 4. The three different sites chosen from M3: C indicates a crater with a diameter of 450 m located in the west of the Chang'E 3 landing site; the spectra of site H and L are the average of the white and yellow box area (20 × 20 pixels), respectively. The mineral abundances of the three regions, H, L, and C, are listed in Table S3.

and the matching results (Table S2) show that the landing site is more olivine rich than the neighboring low-Ti unit. Furthermore, the 450 m impact crater C near the landing site has a similar spectrum with that of the low-Ti unit, implying that this crater may have excavated the underlying low-Ti materials. Since the excavation depth of a 450 m crater is typically smaller than 45 m [*Melosh*, 1989], the thickness of this young high-Ti unit may be less than 45 m.

Since the landing site is a relatively young mare unit and both the VNIS and APXS measurements were performed on the fresh ejecta blanket of a 450 m diameter impact crater, the measurement results may reveal the compositions of the basalts underneath. Both the VNIS and APXS results indicate that the basalt at the landing site has a higher OLV than the surrounding mare unit, suggesting the basalt might be from high-degree partial melting of the deep mantle based on the lunar magma ocean model [*Warren*, 1985]. Furthermore, the basalt has high Al_2O_3 (~11 wt %), FeO, and TiO_2 that is very different than those previously discovered in the returned sample collection [*Lucey et al.*, 2006] and extends the range of basalt types on the Moon [*Neal et al.*, 2015]. The basalts with high aluminum and high OLV are only known from very ancient samples from Apollo 14 [*Shearer et al.*, 2006; *Neal et al.*, 2015]. However, the basalt at the landing site is clearly young (~2.93–2.5 Ga) [*Qiao et al.*, 2014; *Xiao et al.*, 2015], indicating that the heat sources that allow partial melting allow a range of compositions to be sampled irrespective of age. It could imply that the lunar mantle is extremely heterogeneous in composition and heating sufficient to partial melt is not tightly coupled to final composition.

Acknowledgments

We thank Liu Bin for clarifications of the VNIS data format and Carle Pieters for helpful discussions. All the Chang'E-3 data used in this work can be obtained from http://www.bao.ac.cn/. This work was supported by the National Natural Science Foundation of China through grants 41071229 and 41276180 and by the Key Research Program of the Chinese Academy of Sciences (KGZD-EW-603).

The Editor thanks Carle Pieters and an anonymous reviewer for their assistance in evaluating this paper.

References

Besse, S., J. Sunshine, M. Staid, J. Boardman, C. Pieters, P. Guasqui, E. Malaret, S. McLaughlin, Y. Yokota, and J.-Y. Li (2013), A visible and near-infrared photometric correction for Moon Mineralogy Mapper (M^3), *Icarus*, *222*, 229–242.

Denevi, B., P. Lucey, and S. Sherman (2008), Radiative transfer modeling of near-infrared spectra of lunar mare soils: Theory and measurement, *J. Geophys. Res.*, *113*, E02003, doi:10.1029/2007JE002929.

Donaldson Hanna, K., I. Thomas, B. Greenhagen, N. Bowles, and C. Pieters (2014), Characterization of Apollo soil samples under simulated lunar conditions, paper presented at Lunar and Planetary Science Conference, The Woodlands, Tex., 17–21 March.

Hapke, B. (2012), *Theory of Reflectance and Emittance Spectroscopy*, Cambridge Univ. Press, Cambridge, U. K.

Jin, W., H. Zhang, Y. Yuan, K. Di, W. Wan, B. Xu, B. Xue, Y. Yang, L. Xiao, and Z. Wang (2015), In-situ lunar phase curves extracted from imageries measured by panorama cameras on board the Yutu rover of Chang'e 3 mission, paper presented at Lunar and Planetary Science Conference, The Woodlands, Tex., 16–20 March.

Liu, B., C.-L. Li, G.-L. Zhang, R. Xu, J.-J. Liu, X. Ren, X. Tan, X.-X. Zhang, W. Zuo, and W.-B. Wen (2014), Data processing and preliminary results of the Chang'e-3 VIS/NIR imaging spectrometer in-situ analysis, *Res. Astron. Astrophys.*, *14*, 1578, doi:10.1088/1674-4527/14/12/007.

Lucey, P. G. (2004), Mineral maps of the Moon, *Geophys. Res. Lett.*, *31*, L08701, doi:10.1029/2003GL019406.

Lucey, P. G., J. A. Norman, S. T. Crites, G. J. Taylor, B. Hawke, M. Lemelin, and H. J. Melosh (2014), A large spectral survey of small lunar craters: Implications for the composition of the lunar mantle, *Am. Mineral.*, *99*, 2251–2257, doi:10.2138/am-2014-4854.

Lucey, P., R. L. Korotev, J. J. Gillis, L. A. Taylor, D. Lawrence, B. A. Campbell, R. Elphic, B. Feldman, L. L. Hood, and D. Hunten (2006), Understanding the lunar surface and space-Moon interactions, *Rev. Mineral. Geochem.*, *60*, 83–219, doi:10.2138/rmg.2006.60.2.

Melosh, H. J. (1989), *Impact Cratering: A Geologic Process, Research Supported by NASA*, *Oxford Monogr. on Geol. and Geophys.*, vol. 11, 253 pp., Oxford Univ. Press, New York.

Neal, C., Y. Wu, X. Cui, W. Peng, and J. Ping (2015), Regolith at the Chang'e-3 landing site: A new type of mare basalt composition, paper presented at Lunar and Planetary Science Conference, The Woodlands, Tex., 16–20 March.

Noble, S. K., C. M. Pieters, T. Hiroi, and L. A. Taylor (2006), Using the modified Gaussian model to extract quantitative data from lunar soils, *J. Geophys. Res.*, *111*, E11009, doi:10.1029/2006JE002721.

Ohtake, M., C. Pieters, P. Isaacson, S. Besse, Y. Yokota, T. Matsunaga, J. Boardman, S. Yamomoto, J. Haruyama, and M. Staid (2013), One Moon, many measurements 3: Spectral reflectance, *Icarus*, *226*, 364–374, doi:10.1016/j.icarus.2013.05.010.

Pieters, C. M., E. M. Fischer, O. Rode, and A. Basu (1993), Optical effects of space weathering: The role of the finest fraction, *J. Geophys. Res.*, *98*, 20,817–20,824, doi:10.1029/93JE02467.

Pieters, C. M., J. Boardman, B. Buratti, A. Chatterjee, R. Clark, T. Glavich, R. Green, J. Head, P. Isaacson, and E. Malaret (2009), The Moon mineralogy mapper (M3) on Chandrayaan-1, *Curr. Sci.*, *96*, 500–505.

Pieters, C., J. Boardman, M. Ohtake, T. Matsunaga, J. Haruyama, R. Green, U. Mall, M. Staid, P. Isaacson, and Y. Yokota (2013), One Moon, many measurements 1: Radiance values, *Icarus*, *226*, 951–963, doi:10.1016/j.icarus.2013.07.008.

Qiao, L., L. Xiao, J. Zhao, Q. Huang, and J. Haruyama (2014), Geological features and evolution history of Sinus Iridum, the Moon, *Planet. Space Sci.*, *101*, 37–52, doi:10.1016/j.pss.2014.06.007.

Shearer, C. K., P. C. Hess, M. A. Wieczorek, M. E. Pritchard, E. M. Parmentier, L. E. Borg, J. Longhi, L. T. Elkins-Tanton, C. R. Neal, and I. Antonenko (2006), Thermal and magmatic evolution of the Moon, *Rev. Mineral. Geochem.*, *60*, 365–518, doi:10.2138/rmg.2006.60.4.

Shkuratov, Y., V. Kaydash, V. Korokhin, Y. Velikodsky, N. Opanasenko, and G. Videen (2011), Optical measurements of the Moon as a tool to study its surface, *Planet. Space Sci.*, *59*, 1326–1371, doi:10.1016/j.pss.2011.06.011.

Staid, M. I., and C. M. Pieters (2001), Mineralogy of the last lunar basalts: Results from Clementine, *J. Geophys. Res.*, *106*, 27,887–27,900, doi:10.1029/2000JE001387.

Staid, M., C. Pieters, S. Besse, J. Boardman, D. Dhingra, R. Green, J. Head, P. Isaacson, R. Klima, and G. Kramer (2011), The mineralogy of late stage lunar volcanism as observed by the Moon Mineralogy Mapper on Chandrayaan-1, *J. Geophys. Res.*, *116*, E00G10, doi:10.1029/2010JE003735.

Thiessen, F., S. Besse, M. I. Staid, and H. Hiesinger (2014), Mapping lunar mare basalt units in Mare Imbrium as observed with the Moon Mineralogy Mapper (M^3), *Planet. Space Sci.*, *104*, 244–252, doi:10.1016/j.pss.2014.10.003.

Warren, P. H. (1985), The magma ocean concept and lunar evolution, *Annu. Rev. Earth Planet. Sci.*, *13*, 201–240.

Xiao, L., P. Zhu, G. Fang, Z. Xiao, Y. Zou, J. Zhao, N. Zhao, Y. Yuan, L. Qiao, and X. Zhang (2015), A young multilayered terrane of the northern Mare Imbrium revealed by Chang'E-3 mission, *Science*, *347*, 1226–1229, doi:10.1126/science.1259866.

Yamamoto, S., T. Matsunaga, Y. Ogawa, R. Nakamura, Y. Yokota, M. Ohtake, J. Haruyama, T. Morota, C. Honda, and T. Hiroi (2011), Preflight and in-flight calibration of the spectral profiler on board SELENE (Kaguya), *IEEE Trans. Geosci. Remote Sens.*, *49*, 4660–4676, doi:10.1109/TGRS.2011.2144990.

Zhao, J., J. Huang, L. Qiao, Z. Xiao, Q. Huang, J. Wang, Q. He, and L. Xiao (2014), Geologic characteristics of the Chang'E-3 exploration region, *Sci. China Phys. Mech. Astron.*, *57*, 569–576.